Chinese Journal of Aeronautics, (2017), 30(5): 1670–1680

Chinese Society of Aeronautics and Astronautics
& Beihang University

Chinese Journal of Aeronautics

cja@buaa.edu.cn
www.sciencedirect.com

Research on parafoil stability using a rapid estimate model

Hua YANG [a], Lei SONG [b,*], Weifang CHEN [a]

[a] School of Aeronautics and Astronautics, Zhejiang University, Hangzhou 310013, China
[b] School of Aeronautic Science and Engineering, Beihang University, Beijing 100083, China

Received 18 July 2016; revised 30 September 2016; accepted 22 November 2016
Available online 20 June 2017

KEYWORDS

Dynamic model;
Motion mode;
Parafoil;
Small-disturbance theory;
Stability

Abstract With the consideration of rotation between canopy and payload of parafoil system, a four-degree-of-freedom (4-DOF) longitudinal static model was used to solve parafoil state variables in straight steady flight. The aerodynamic solution of parafoil system was a combination of vortex lattice method (VLM) and engineering estimation method. Based on small disturbance assumption, a 6-DOF linear model that considers canopy additional mass was established with benchmark state calculated by 4-DOF static model. Modal analysis of a dynamic model was used to calculate the stability parameters. This method, which is based on a small disturbance linear model and modal analysis, is high-efficiency to the study of parafoil stability. It is well suited for rapid stability analysis in the preliminary stage of parafoil design. Using this method, this paper shows that longitudinal and lateral stability will both decrease when a steady climbing angle increases. This explains the wavy track of the parafoil observed during climbing.

© 2017 Production and hosting by Elsevier Ltd. on behalf of Chinese Society of Aeronautics and Astronautics. This is an open access article under the CC BY-NC-ND license (http://creativecommons.org/licenses/by-nc-nd/4.0/).

1. Introduction

The stability of a parafoil is a significant research field because it is a very important component of flying quality. The stability and the maneuverability of the parafoil were studied by Goodrick in his early literatures.[1–3] He established a longitudinal three-degree-of-freedom (3-DOF) model in 1975. Using tunnel data, the longitudinal static and dynamic stability of the parafoil system were analyzed with the help of the 3-DOF dynamic model. Before long, Goodrick built a 6-DOF model to evaluate the parafoil's dynamic stability and to simulate the response with flap controls. Using the same dynamic model, Goodrick explored how scale affected the dynamic characteristics of a parafoil.

In the 1970s, Nicolaides collected and organized a comprehensive set of parafoil wind tunnel data that was used in the research of flight performance, static stability, and maneuverability.[4,5] In 2007, Redelinghuys and Rhodes focused attention on other analysis methods, which can show the trim state and static stability graphically in pictures.[6] The other studies on parafoil stability were either about static stability or based on dynamic simulation.[7–11] Parafoil static stability analysis

* Corresponding author.
E-mail address: songlei@buaa.edu.cn (L. SONG).

Peer review under responsibility of Editorial Committee of CJA.

Production and hosting by Elsevier

http://dx.doi.org/10.1016/j.cja.2017.06.003
1000-9361 © 2017 Production and hosting by Elsevier Ltd. on behalf of Chinese Society of Aeronautics and Astronautics.
This is an open access article under the CC BY-NC-ND license (http://creativecommons.org/licenses/by-nc-nd/4.0/).

was a rapid and intuitive method, but it can only give the motional tendency of the parafoil after a disturbance. Although dynamic simulation can simulate all the motor processes with which the motion convergence can be judged, it needs complex numerical calculations without any quantitative parameter.[12–17]

In this paper, a longitudinal static model was used for solving parafoil state variables in a steady straight flight. This model has four degrees of freedom in the longitudinal plane due to the consideration of the relative motion between the canopy and the payload. Small disturbance linear equations were also presented to analyze the stability of the parafoil in a steady straight flight. The longitudinal and lateral stability will worsen when the steady climbing angle becomes larger. The conclusion nicely supports the phenomenon of decreased stability that occurs during climbing in test flights of a powered parafoil. The relative position between the canopy and the payload significantly affects the stability of the whole system.

2. Analysis model

2.1. Summary of parafoil system

A powered parafoil with a NACA4415 airfoil and a rectangular flat shape was studied in this paper. The mass of its payload is 1 kg. All suspension lines joined to two bilateral symmetry points, collectively named J_1, at the end. Through two ropes, point J_1 was connected to the payload lashing points named J_2. The electrical motor-propeller system on the cylindrical payload provided the driving force T for the parafoil. Because the canopy remained tight during most of the time in motion, the barycenter of the canopy was replaced by a fixed point O_1. The point O_2 was regarded as the barycenter of the payload. The mass of the suspension lines was ignored because of their small value. All sizes of the parafoil system are shown in Fig. 1 and are explained in Table 1.

2.2. Model of aerodynamic force

Aerodynamic force was divided into the following three parts to be calculated. Lift and induced drag were solved by numerical method based on potential flow theory. Drag independent of lift was calculated by an engineering estimation. Additional mass force was also estimated by an engineering method.

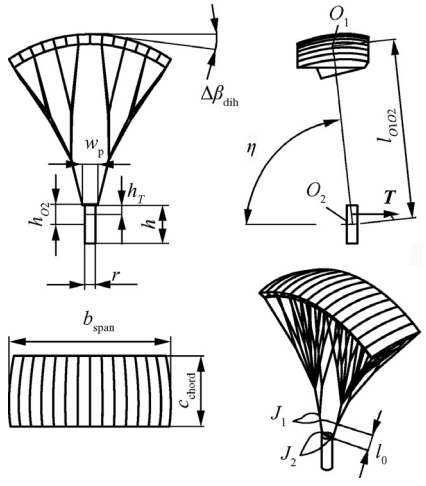

Fig. 1 Geometric profile of a parafoil.

Table 1 Parameters of parafoil.

Meaning of symbol	Value
Distance between two barycenters of canopy and payload l_{O1O2} (m)	2
Angle between l_{O1O2} and airfoil chord line η (°)	75
Length of airfoil chord c_{chord} (m)	0.7
Length of wing span b_{span} (m)	1.5
Inlet height of open airfoil nose h_{inlet} (m)	0.07
Dihedral between adjacent sections $\Delta\beta_{dih}$ (°)	5
Height of payload h (m)	0.4
Diameter of payload d (m)	0.1
Distance between two lashing points on payload w_p (m)	0.2
Vertical distance between driving force and lashing point on payload h_T (m)	0.12
Vertical distance between payload barycenter and lashing point on payload h_{O2} (m)	0.3
Length of single rope between J_1 and J_2 (J_1 and J_2 are joint points of suspension lines shown in Fig. 1) l_0 (m)	0.1
Canopy areal density ρ (kg/m^2)	0.09

2.2.1. Lift and induced drag

Due to the inflated canopy and the tight suspension lines, the whole parafoil system could be regarded as a rigid body in steady flight. There were two properties of the flow field around the parafoil. First, the flow field without large separation was very similar to that of a normal airfoil at a small angle of attack. Second, there was almost no airflow inside the canopy after its inflation.

Because of the potential flow around the canopy and the isolation between the inside and outside of the canopy, the vortex lattice method (VLM) was applied to solving the lift and induced drag of the canopy.

Lift, induced drag and other relevant moments were calculated using the open source program Tornado coded by Melin.[18] Similar open source program was also effectively used by Song lei in his dynamic stability research on low speed aircraft.[19,20]

2.2.2. Other types of drag

In addition to the induced drag, the parafoil drag also contained canopy zero lift drag coefficient C_{D0}, suspension line drag coefficient C_{Dl}, and payload drag coefficient C_{Dp}.

(1) Canopy zero lift drag coefficient C_{D0}

Basic airfoil drag, surface irregularities and fabric roughness, open airfoil nose, and drag of pennants and stabilizer panels were all zero lift drag sources.[21] A detailed list is included in Table 2.

(2) Suspension line drag coefficient C_{Dl}

Because every suspension line has a cylindrical shape, the drag coefficient, whose reference area is the windward area, was approximately equal to 1 if the Reynolds

Table 2 Components of canopy zero lift drag coefficient.

Zero lift drag type	Drag coefficient
Basic airfoil drag	0.015
Surface irregularities and fabric roughness	0.004
Open airfoil nose	$0.5h_{\text{inlet}}/c_{\text{chord}} = 0.05$
Drag of pennants and stabilizer panels	0.001

number was in the range of 100–100000. Therefore, the usual sense drag coefficient, whose reference area is wing area, can be calculated as follows:

$$C_{Dl} = \frac{A_l}{S} \tag{1}$$

where A_l is the projected area of suspension lines in the direction of incoming flow, and S the canopy area.

(3) Payload drag coefficient C_{Dp}
The drag coefficient estimation method of payload is the same as that of the suspension lines because of the cylinder-shaped payload. The drag coefficient of payload can be calculated as follows:

$$C_{Dp} = \frac{A_p}{S} \tag{2}$$

where A_p is the projected area of payload in the direction of incoming flow.

2.2.3. Apparent mass force

The apparent mass has a strong effect on the flight dynamics of lightly loaded flight vehicles such as parafoils. It is always expressed as a 6-order matrix, which includes 3 translational mass elements, 3 rotational inertia elements and several coupled elements. If a body has three orthogonal symmetry planes such as a spheroid, its apparent mass matrix can be simplified to 3 translational mass elements and 3 rotational inertia elements. These simplified elements generally come as m_A, m_B, m_C, I_A, I_B, I_C (Fig. 2, a is the height of canopy arch, b is the length of canopy span, c is the airfoil chord length, t_a is the airfoil thickness). 'u, v, w' and 'p, q, r' are translational and rotational velocities of ellipsoidal canopy in the direction of 'X, Y, Z' axis. Kinetic energy of canopy apparent mass E is shown as Eq. (3), while impulse and impulsive moment of apparent mass $\boldsymbol{I}_F$ and $\boldsymbol{I}_M$ are presented as Eq. (4). Apparent forces and moments acting on canopy are expressed as Eq. (5).

$$E = \frac{1}{2}\left(m_A u^2 + m_B v^2 + m_C w^2 + I_A p^2 + I_B q^2 + I_C r^2\right) \tag{3}$$

$$\begin{cases} \boldsymbol{I}_F = \left[\dfrac{\partial E}{\partial u}\ \dfrac{\partial E}{\partial v}\ \dfrac{\partial E}{\partial w}\right]^{\mathrm{T}} = [m_A u \quad m_B v \quad m_C w]^{\mathrm{T}} \\ \boldsymbol{I}_M = \left[\dfrac{\partial E}{\partial p}\ \dfrac{\partial E}{\partial q}\ \dfrac{\partial E}{\partial r}\right]^{\mathrm{T}} = [I_A p \quad I_B q \quad I_C r]^{\mathrm{T}} \end{cases} \tag{4}$$

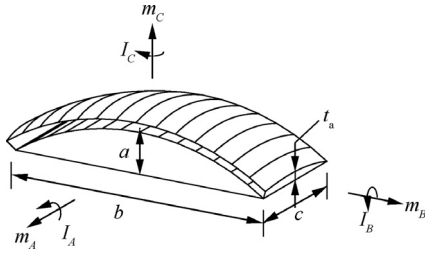

Fig. 2 Definition of canopy apparent mass.

$$\begin{cases} \boldsymbol{F}_{\text{app}} = -\dfrac{\mathrm{d}\boldsymbol{I}_F}{\mathrm{d}t} = -\dfrac{\partial \boldsymbol{I}_F}{\partial t} - \boldsymbol{\omega} \times \boldsymbol{I}_F \\ \boldsymbol{M}_{\text{app},0} = -\dfrac{\mathrm{d}\boldsymbol{I}_M}{\mathrm{d}t} = -\dfrac{\partial \boldsymbol{I}_M}{\partial t} - \boldsymbol{\omega} \times \boldsymbol{I}_M \\ \boldsymbol{\omega} = [p \quad q \quad r]^{\mathrm{T}} \end{cases} \tag{5}$$

The expanded form of Eq. (5) is as follows:

$$\begin{cases} \boldsymbol{F}_{\text{app}} = \begin{bmatrix} -m_A\dot{u} - qwm_C + rvm_B \\ -m_B\dot{v} - rum_A + pwm_C \\ -m_C\dot{w} - pvm_B + qum_A \end{bmatrix} \\ \boldsymbol{M}_{\text{app},0} = \begin{bmatrix} -I_A\dot{p} - qr(I_C - I_B) \\ -I_B\dot{q} - pr(I_A - I_C) \\ -I_C\dot{r} - pq(I_B - I_A) \end{bmatrix} \end{cases} \tag{6}$$

where $\boldsymbol{F}_{\text{app}}$ is the canopy apparent force, $\boldsymbol{M}_{\text{app},0}$ the canopy apparent moment. For a briefer dynamic model, the canopy is regarded as a spheroid while the apparent mass is considered.

Lissaman proposed an engineering estimation method for the parafoil apparent mass with the assumption of a spheroid canopy.[22] This method expresses the canopy apparent mass matrix by 4 geometric parameters including wing span 'b', canopy arch height 'a', chord length 'c' and airfoil thickness 't_a'. With the consideration of the canopy geometrical factors, this estimation method has acceptable accuracy and speed and is used in the following dynamic modeling. All geometric parameters and apparent mass results are presented in Table 3.

$$\begin{cases} m_A = 0.666\left[1 + \dfrac{8}{3}\left(\dfrac{a}{b}\right)^2\right] t_a^2 b\rho \\ m_B = 0.267\left\{t_a^2 + 2a^2\left[1 - \left(\dfrac{t_a}{b}\right)^2\right]\right\} c\rho \\ m_C = 0.785\left\{1 + 2\left(\dfrac{a}{b}\right)^2\left[1 - \left(\dfrac{t_a}{b}\right)^2\right]\right\}^{1/2} \dfrac{A}{1+A} bc^2\rho \\ I_A = 0.055\dfrac{A}{1+A} bs^2\rho \\ I_B = 0.0308\dfrac{A}{1+A}\left[1 + \dfrac{\pi}{6}(1+A)A\left(\dfrac{a}{b}\right)^2\left(\dfrac{t_a}{c}\right)^2\right] c^3 s\rho \\ I_C = 0.0555\left[1 + 8\left(\dfrac{a}{b}\right)^2\right] b^3 t_a^2\rho \\ A = \dfrac{b}{c} \\ s = bc \end{cases} \tag{7}$$

Table 3 Canopy geometric parameters and apparent mass.

Parameter	Value
a (m)	0.138
b (m)	1.57
c (m)	0.7
t_a (m)	0.105
m_A (kg)	0.0172
m_B (kg)	0.0134
m_C (kg)	0.6153
I_A (kg m^2)	0.1095
I_B (kg m^2)	0.0120
I_C (kg m^2)	0.0037

2.3. Dynamic model

A parafoil stability study is always based on a steady flight status and focuses on the motional process after a small disturbance where the parafoil deformation is very small. However, the relative position of the canopy and the payload change a lot between the different steady flight statuses of a parafoil. In view of the above-mentioned facts, first, a 4-DOF static model which includes relative rotation between canopy and payload is used to solve steady flight status parameters. Then, 6-DOF dynamic model for a rigid body is used to study the parafoil motion after a small disturbance.

The earth rotation, earth curvature, atmosphere wind field and mass of suspension lines are all ignored in the following modeling process.

2.3.1. Coordinate system

There are 5 right-handed coordinate systems in this paper, including ground axes, parafoil axes, canopy axes, payload axes, and wind axes. The definitions of axes are included in Table 4.

2.3.2. 4-DOF longitudinal static model

The relative rotational angle between the canopy and the payload significantly differs with different straight flight statuses.[23] There are 4 parameters to solve in a 4-DOF static model (Fig. 3), including the angle of attack α, engine thrust $\boldsymbol{T}$, flight speed $\boldsymbol{V}$, and relative rotation between canopy and payload $\Delta\theta$. Because the canopy and the suspension lines are tight while in steady flight, the rotation reference point of the canopy and the payload can be chosen at point J_2 and point J_1. To solve the 4 state variables (α, $\boldsymbol{T}$, $\boldsymbol{V}$, $\Delta\theta$), 4 equilibrium equations are proposed as follows:

Table 4 Coordinate system of dynamic model.

Axes	Coordinate system's origin	X-axis	Z-axis
Ground axes ($O_gX_gY_gZ_g$)	O_g: initial position of parafoil system barycenter	Parallel to initial course and horizontal plane	Downward in vertical direction
Parafoil axes ($O_bX_bY_bZ_b$)	O_b: parafoil system barycenter	Parallel to airfoil chord line on symmetry plane	Perpendicular to Axis X_b on symmetry plane
Canopy axes ($O_1X_{b1}Y_{b1}Z_{b1}$)	O_1: canopy barycenter	Parallel to airfoil chord line on symmetry plane	Perpendicular to axis X_{b1} on symmetry plane
Payload axes ($O_2X_{b2}Y_{b2}Z_{b2}$)	O_2: payload barycenter	Forward axis of payload	Perpendicular to axis X_{b2} on symmetry plane
Wind axes ($O_aX_aY_aZ_a$)	O_a: parafoil system barycenter	Parallel to velocity direction	Perpendicular to axis X_a on symmetry plane

$$\begin{cases} \boldsymbol{L}+\boldsymbol{D}_1+\boldsymbol{D}_{sl}+\boldsymbol{G}_1+\boldsymbol{G}_{s1}+\boldsymbol{T}+\boldsymbol{D}_2+\boldsymbol{G}_2=\boldsymbol{0} \\ M_{\boldsymbol{L},J_1}+M_{\boldsymbol{D}_1,J_1}+M_{\boldsymbol{D}_{sl},J_1}+M_{\boldsymbol{G}_1,J_1}+M_{\boldsymbol{G}_{sl},J_1}+M_0=0 \\ M_{\boldsymbol{T},J_2}+M_{\boldsymbol{D}_2,J_2}+M_{\boldsymbol{G}_2,J_2}=0 \end{cases} \tag{8}$$

where $\boldsymbol{L}$ is the canopy lift, $\boldsymbol{D}_1$ the canopy drag, $\boldsymbol{D}_2$ the payload drag, $\boldsymbol{D}_{sl}$ the drag of suspension lines, $\boldsymbol{G}_1$ the canopy gravity, $\boldsymbol{G}_2$ the payload gravity, $\boldsymbol{G}_{sl}$ the gravity of suspension lines.

The first vector expression of Eq. (8) contains 2 equilibrium equations in X-axis and Z-axis directions. The left two expressions of Eq. (8) show the moment balances of canopy-line system and payload system. Symbols like '$M_{\boldsymbol{A},B}$' mean a moment of force $\boldsymbol{A}$ on reference point B.

Based on the 4-DOF static model, a particular engine thrust leads to a group of state variables (α, $\boldsymbol{T}$, $\boldsymbol{V}$, $\Delta\theta$), which results in the stability characteristics of a parafoil.

2.3.3. 6-DOF dynamic model

Because the stability characteristics are always analyzed with the assumption of a small disturbance based on a certain equilibrium state, the canopy deformation and the relative rotation between the canopy and the payload are too small to be considered. Therefore, the following stability research model is derived from the 6-DOF dynamic model of a rigid body.

The 6-DOF dynamic model always contains the following equation sets (Eqs. (10)–(13)), including the translational dynamic equation set, rotational dynamic equation set, rotational kinematic equation set and translational kinematic equation set.

$$\begin{cases} m\dfrac{\mathrm{d}\boldsymbol{V}_p}{\mathrm{d}t}=\boldsymbol{F}_{app}+\boldsymbol{F}_{aero}+\boldsymbol{G} \\ \dfrac{\mathrm{d}\boldsymbol{H}}{\mathrm{d}t}=\boldsymbol{M}_{app,0}+\boldsymbol{F}_{app}\times\boldsymbol{O}_1\boldsymbol{O}_b+\boldsymbol{M}_{aero} \end{cases} \tag{9}$$

$$\begin{bmatrix} (m+m_A)\dot{u} \\ (m+m_B)\dot{v} \\ (m+m_C)\dot{w} \end{bmatrix} = \begin{bmatrix} rv(m+m_B)-qw(m+m_C) \\ pw(m+m_C)-ru(m+m_A) \\ qu(m+m_A)-pv(m+m_B) \end{bmatrix} + \begin{bmatrix} X \\ Y \\ Z \end{bmatrix} + \begin{bmatrix} -mg\sin\theta \\ mg\sin\phi\cos\theta \\ mg\cos\phi\cos\theta \end{bmatrix} \tag{10}$$

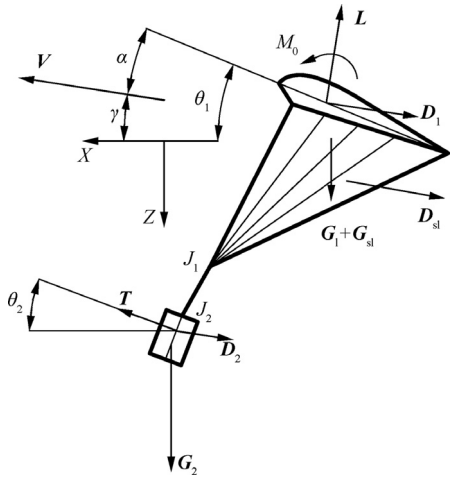

Fig. 3 4-DOF static model.

$$\begin{bmatrix} \dot{p}I_X+\dot{p}I_A-\dot{r}I_{ZX}+qr(I_Z-I_Y+I_C-I_B)-pqI_{ZX} \\ \dot{q}I_Y+\dot{q}I_B+pr(I_X-I_Z+I_A-I_C)-r^2I_{ZX}+p^2I_{ZX} \\ \dot{r}I_Z+\dot{r}I_C-\dot{p}I_{ZX}+pq(I_Y-I_X+I_B-I_A)+qrI_{ZX} \end{bmatrix} - \begin{bmatrix} (-m_B\dot{v}-rum_A+pwm_C)Z_1 \\ (-m_C\dot{w}-pvm_B+qum_A)X_1-(-m_A\dot{u}-qwm_C+rvm_B)Z_1 \\ (m_B\dot{v}+rum_A-pwm_C)X_1 \end{bmatrix} = \begin{bmatrix} L \\ M \\ N \end{bmatrix} \tag{11}$$

$$\begin{bmatrix} \dot{\phi} \\ \dot{\theta} \\ \dot{\psi} \end{bmatrix} = \begin{bmatrix} 1 & \sin\phi\tan\theta & \cos\phi\tan\theta \\ 0 & \cos\phi & -\sin\phi \\ 0 & \sin\phi\sec\theta & \cos\phi\sec\theta \end{bmatrix} \begin{bmatrix} p \\ q \\ r \end{bmatrix} \tag{12}$$

$$\begin{bmatrix} \dot{X} \\ \dot{Y} \\ \dot{Z} \end{bmatrix} = \begin{bmatrix} \cos\theta\cos\psi & \sin\phi\sin\theta\cos\psi-\cos\phi\sin\psi & \cos\phi\sin\theta\cos\psi+\sin\phi\sin\psi \\ \cos\theta\sin\psi & \sin\phi\sin\theta\sin\psi+\cos\phi\cos\psi & \cos\phi\sin\theta\sin\psi-\sin\phi\cos\psi \\ -\sin\theta & \sin\phi\cos\theta & \cos\phi\cos\theta \end{bmatrix} \begin{bmatrix} u \\ v \\ w \end{bmatrix} \tag{13}$$

where $\boldsymbol{V}_{\mathrm{p}}$ is the parafoil velocity, $\boldsymbol{H}$ the parafoil angular momentum, $\boldsymbol{G}$ the parafoil gravity, $\boldsymbol{F}_{\mathrm{aero}}$ the aerodynamic force of parafoil, $\boldsymbol{M}_{\mathrm{aero}}$ the aerodynamic moment of parafoil, $\boldsymbol{O}_1\boldsymbol{O}_{\mathrm{b}}$ the geometric vector from point O_1 to point O_{b}, ϕ the roll angle of parafoil, θ the pitch angle of parafoil, ψ the yaw angle of parafoil, L the rolling moment of parafoil, M the pitching moment of parafoil, N the yawing moment of parafoil.

2.4. Model of stability analysis

2.4.1. Small disturbance linear equations

Parafoil dynamic equations are very limited except for the numerical method that easily simulates the movement process, but the stability parameters are difficult to find. The linear dynamic model, which is based on a small disturbance theory, contains certain stability parameters solved from the eigen matrix. With quantitative parameters, the stability analysis and parafoil design can be more precise and visual.

Eq. (13) and the last formula of Eq. (12) are independent from the parafoil dynamic model, so there are 8 formulas to be linearized with 8 small disturbance variables including Δu, Δv, Δw, Δp, Δq, Δr, $\Delta\phi$ and $\Delta\theta$. Because the base state is a steady straight flight, all the lateral variables are zeros at the very start, such as $v_0 = 0$, $p_0 = 0$, $q_0 = 0$, $r_0 = 0$ and $\phi_0 = 0$. The disturbance variables of aerodynamic forces are linearized in Eq. (14). Although the stability characteristics are focused, the control inputs, such as engine throttle change or control surface deflection, are discounted in the linear dynamic model (Eqs. (15) and (16)).

$$\begin{cases} \Delta X = X_u\Delta u + X_w\Delta w + X_q\Delta q \\ \Delta Y = Y_v\Delta v + Y_p\Delta p + Y_r\Delta r \\ \Delta Z = Z_u\Delta u + Z_w\Delta w + Z_q\Delta q \\ \Delta L = L_v\Delta v + L_p\Delta p + L_r\Delta r \\ \Delta M = M_u\Delta u + M_w\Delta w + M_q\Delta q \\ \Delta N = N_v\Delta v + N_p\Delta p + N_r\Delta r \end{cases} \tag{14}$$

$$\begin{bmatrix} \Delta\dot{u} \\ \Delta\dot{w} \\ \Delta\dot{q} \\ \Delta\dot{\theta} \end{bmatrix} = \boldsymbol{A}_{\mathrm{lon}} \begin{bmatrix} \Delta u \\ \Delta w \\ \Delta q \\ \Delta\theta \end{bmatrix} \tag{15}$$

$$\begin{bmatrix} \Delta\dot{v} \\ \Delta\dot{p} \\ \Delta\dot{r} \\ \Delta\dot{\phi} \end{bmatrix} = \boldsymbol{A}_{\mathrm{lat}} \begin{bmatrix} \Delta v \\ \Delta p \\ \Delta r \\ \Delta\phi \end{bmatrix} \tag{16}$$

$$\begin{cases} \boldsymbol{A}_{\mathrm{lon}} = \boldsymbol{P}_{\mathrm{lon}}^{-1}\boldsymbol{Q}_{\mathrm{lon}} \\ \boldsymbol{A}_{\mathrm{lat}} = \boldsymbol{P}_{\mathrm{lat}}^{-1}\boldsymbol{Q}_{\mathrm{lat}} \end{cases} \tag{17}$$

$$\begin{cases} \boldsymbol{P}_{\mathrm{lon}} = \begin{bmatrix} m+m_A & 0 & 0 & 0 \\ 0 & m+m_C & 0 & 0 \\ -m_AZ_1 & m_CX_1 & I_Y+I_B & 0 \\ 0 & 0 & 0 & 1 \end{bmatrix} \\ \boldsymbol{Q}_{\mathrm{lon}} = \begin{bmatrix} X_u & X_w & X_q-w_0(m+m_C) & -mg\cos\theta_0 \\ Z_u & Z_w & Z_q+u_0(m+m_A) & -mg\sin\theta_0 \\ M_u & M_w & M_q+(u_0m_AX_1+w_0m_CZ_1) & 0 \\ 0 & 0 & 1 & 0 \end{bmatrix} \end{cases} \tag{18}$$

$$\begin{cases} \boldsymbol{P}_{\mathrm{lat}} = \begin{bmatrix} m+m_B & 0 & 0 & 0 \\ m_BZ_1 & I_X+I_A & -I_{ZX} & 0 \\ -m_BX_1 & -I_{ZX} & I_Z+I_C & 0 \\ 0 & 0 & 0 & 1 \end{bmatrix} \\ \boldsymbol{Q}_{\mathrm{lat}} = \begin{bmatrix} Y_v & Y_p+w_0(m+m_C) & Y_r-u_0(m+m_A) & mg\cos\theta_0 \\ L_v & L_p+w_0m_CZ_1 & L_r-u_0m_AZ_1 & 0 \\ N_v & N_p-w_0m_CX_1 & N_r+u_0m_AX_1 & 0 \\ 0 & 1 & \tan\theta_0 & 0 \end{bmatrix} \end{cases} \tag{19}$$

where X_1 is the X-coordinate of $\boldsymbol{O}_1\boldsymbol{O}_{\mathrm{b}}$ on parafoil axes, Y_1 the Y-coordinate of $\boldsymbol{O}_1\boldsymbol{O}_{\mathrm{b}}$ on parafoil axes, Z_1 the Z-coordinate of $\boldsymbol{O}_1\boldsymbol{O}_{\mathrm{b}}$ on parafoil axes.

Eqs. (15) and (16) are linear ordinary differential equations with constant coefficients that have well-developed theories for analytical solutions and equation characteristics. Therefore, the linear dynamic model, which is always separated into a longitudinal model and a lateral model, is significant for dynamic analysis, conceptual design and flight control.

2.4.2. Modal analysis

According to the linear ordinary differential equation theory, the linear dynamic modal characteristics of a parafoil can be analyzed as follows. The longitudinal linear dynamic model is used as an example.

The solution of Eq. (15) is as follows:

$$\begin{bmatrix}\Delta u(t)\\ \Delta w(t)\\ \Delta q(t)\\ \Delta\theta(t)\end{bmatrix} = C_1\boldsymbol{x}_1 e^{\lambda_1 t} + C_2\boldsymbol{x}_2 e^{\lambda_2 t} + C_3\boldsymbol{x}_3 e^{\lambda_3 t} + C_4\boldsymbol{x}_4 e^{\lambda_4 t} \tag{20}$$

The longitudinal disturbance motion is composed of 4 exponential functions. C_i is constant, and $\boldsymbol{x}_i$ is eigenvector. λ_i is the eigenvalue of matrix $\boldsymbol{A}_{\text{lon}}$ whose eigenvalue may be a real root or a complex root. When the eigenvalue is a real number, the corresponding mode is monotonic, and the negative real root leads to a convergent property. When the eigenvalues are a pair of conjugate complex numbers, the corresponding mode is periodic, and the negative real part leads to a convergent property.

$$\lambda_{i,j} = \xi \pm \mathrm{i}\omega \tag{21}$$

where ξ is the real part of eigenvalue, ω the imaginary part of eigenvalue.

$$\begin{cases} t_{\text{half}} = -\ln\dfrac{2}{\lambda} & \text{Monotonic convergence}\\ t_{\text{half}} = -\ln\dfrac{2}{\xi} & \text{Oscillatory convergence}\\ t_{\text{double}} = \ln\dfrac{2}{\lambda} & \text{Monotonic divergence}\\ t_{\text{double}} = \ln\dfrac{2}{\xi} & \text{Oscillatory divergence}\end{cases} \tag{22}$$

where t_{half} is the half-life time, and t_{double} the time to double amplitude.

The relationship of frequency ω and period T is as follows:

$$T = \frac{2\pi}{\omega} \tag{23}$$

The convergence property of a mode depends on the real part of its eigenvalue. Negative means convergence and positive means divergence. The larger absolute value of the real part leads to a quicker oscillation frequency.

3. Example analysis

The full process of the stability analysis of the aforementioned parafoil in this paper is as follows (Fig. 4). First, the state parameters are solved on a certain steady straight flight status, which is regarded as a benchmark status by the parafoil 4-DOF static model. Second, the longitudinal and lateral linear dynamic models are deduced from the 6-DOF nonlinear dynamic model with the assumption of a small disturbance near the steady straight flight status. Finally, the longitudinal and lateral modal eigenvalues and characteristics are analyzed using the well-developed theory of linear systems.

Tables 5–8 show the modal eigenvalues and the modal characteristic parameters of every mode. Figs. 5 and 6 propose the variation tendency of modal eigenvalues after the climbing angle. The directions of the arrows display the increasing climbing angle.

The parafoil dynamic modal characteristics include two longitudinal modes and three lateral modes and are very similar to those of fixed-wing airplanes. In most cases, the longitudinal coefficient matrix has two pairs of conjugate complex roots that correspond to two motion modes. One mode, which is named longitudinal mode 1, has a shorter period and converges faster, whereas the other, which is named mongitudinal mode 2, has a longer period and converges slower. In addition, the lateral coefficient matrix has one pair of conjugate complex roots and two real roots. The conjugate complex roots correspond to an oscillation mode which has a shorter period and converges faster, named lateral mode 1. Two real roots mean two monotonous modes, including one fast convergence mode named lateral- mode 2 and one slow convergence mode named lateral mode 3.

Longitudinal mode 2 diverges when the climbing angle increases just like the eigenvalues going across the imaginary axis. When the climbing angle grows, lateral mode 1 and lateral mode 2 slightly change. However, the divergence critical point of lateral mode 3 comes during the gliding to level cruising period, and the divergence speed increases with the climb-

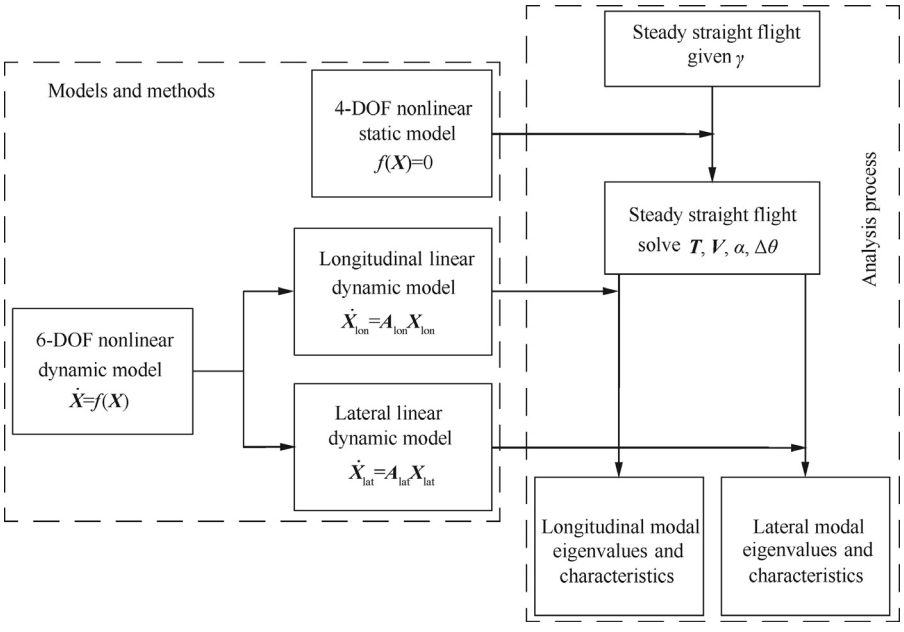

Fig. 4 Process and models of stability analysis.

Table 5 Modal characteristics of longitudinal mode 1.

Climbing angle (°)	Longitudinal mode 1	Period (s)	Half-life time/time to double amplitude (s)
−10	−6.971 ± 3.904i	1.61	0.099
−5	−7.223 ± 4.304i	1.46	0.096
0	−7.486 ± 4.496i	1.40	0.093
5	−7.746 ± 4.495i	1.40	0.089
10	−7.991 ± 4.300i	1.46	0.087
15	−8.217 ± 3.893i	1.61	0.084
20	−8.432 ± 3.196i	1.97	0.082
25	−8.684 ± 1.838i	3.42	0.080

Table 6 Modal characteristics of longitudinal mode 2.

Climbing angle (°)	Longitudinal mode 2	Period (s)	Half-life time/time to double amplitude (s)
−10	−0.432 ± 0.685i	9.17	1.61
−5	−0.385 ± 0.657i	9.57	1.80
0	−0.329 ± 0.634i	9.92	2.10
5	−0.266 ± 0.613i	10.26	2.61
10	−0.196 ± 0.590i	10.65	3.53
15	−0.121 ± 0.562i	11.17	5.75
20	−0.039 ± 0.525i	11.97	17.77
25	0.047 ± 0.471i	13.35	14.81

Table 7 Modal characteristics of lateral mode 1.

Climbing angle (°)	Lateral mode 1	Period (s)	Half-life time/time to double amplitude (s)
−10	−0.699 ± 4.416i	1.423	0.992
−5	−0.776 ± 4.571i	1.375	0.894
0	−0.847 ± 4.681i	1.342	0.818
5	−0.911 ± 4.747i	1.324	0.761
10	−0.964 ± 4.768i	1.318	0.719
15	−1.004 ± 4.746i	1.324	0.690
20	−1.030 ± 4.689i	1.340	0.673
25	−1.040 ± 4.600i	1.366	0.666

ing angle. This explains why the parafoil lateral stability becomes worse during climbing.

In conclusion, the parafoil stability generally worsens when the climbing angle increases, especially in the lateral direction.

4. Model discussion

4.1. Aerodynamic accuracy

A parafoil which has been tested in wind tunnel by NASA Langley Laboratory (Fig. 7) was used to validate the aerodynamic estimation model. The geometric parameters of validation model are as follows.

The aerodynamic estimation method of parafoil in this paper is a combination of vortex lattice method (VLM) and engineering estimation method (EEM). Lift and induced drag of canopy were calculated by VLM, while other types of drag were estimated by EEM. Computational results and wind tunnel data are presented in Figs. 8 and 9.

Though the aerodynamic estimation method in this paper contains some errors, the computational results fit experimental results well, especially at small angles of attack. The computational results can be used in dynamic simulation, even though canopy stall cannot be simulated by this method.

4.2. Computation speed

The mixture of VLM and EEM improved the computational efficiency of parafoil aerodynamic estimation. Computation of 8 modal analysis results took less than 8 s on a common personal computer (CPU: Inter Core i7-4710MQ 2.5 GHz, RAM: 12 GB). Stability analysis model in this paper has an efficient speed, which is very important in conceptual design and optimization iteration.

4.3. Basis of stability analysis model

Stability analysis process in this paper is as follows (Fig. 10):

(1) Assume a parafoil which is in a steady straight flight. All parameters can be calculated by 4-DOF static model including relative angle of canopy and payload.
(2) Movement after small disturbance is the basement of stability analysis. Since the disturbance is weak, the disturbed motion will not cause large relative motion between canopy and payload. Therefore whole parafoil system was regarded as a rigid body whose motion could be described by a 6-DOF dynamic model.
(3) With an assumption of small disturbance, a 6-DOF dynamic model can be simplified into a linear dynamic model which is convenient for stability analysis.

Table 8 Modal characteristics of lateral mode 2 and lateral mode 3.

Climbing angle (°)	Lateral mode 2	Lateral mode 3	Half-life time/time to double amplitude (s)	
			Lateral mode 2	Lateral mode 3
−10	−3.410	−0.179	0.2033	3.88
−5	−3.336	−0.086	0.2078	8.11
0	−3.276	0.014	0.2116	49.51
5	−3.231	0.120	0.2145	5.80
10	−3.202	0.231	0.2164	3.00
15	−3.188	0.350	0.2174	1.98
20	−3.198	0.477	0.2167	1.45
25	−3.230	0.616	0.2146	1.12

5. Geometric influence of parafoil stability

When the climbing angle increases, the parafoil stability will worsen in both longitudinal and lateral directions. Lateral mode 3, in particular, may diverge very quickly. To improve the quality of the parafoil stability, three geometric parameters will be changed and analyzed. These parameters include the centroid distance of the canopy and the payload l_{O1O2}, the angle between the horizontal and the connection line of the canopy and the payload centroids η, and the dihedral of the adjacent air-rooms $\Delta\beta_{\text{dih}}$.

5.1. Relative position of canopy and payload

The relative positions of the canopy and the payload are replaced by two parameters including the centroid distance of the canopy and the payload l_{O1O2} and the angle between the horizontal and the connection line of the canopy and payload centroids η.

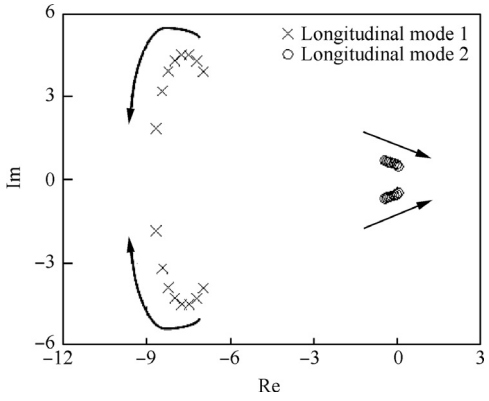

Fig. 5 Root locus of longitudinal modes.

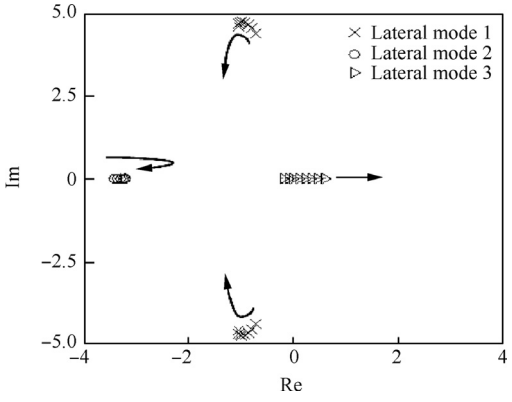

Fig. 6 Root locus of lateral modes.

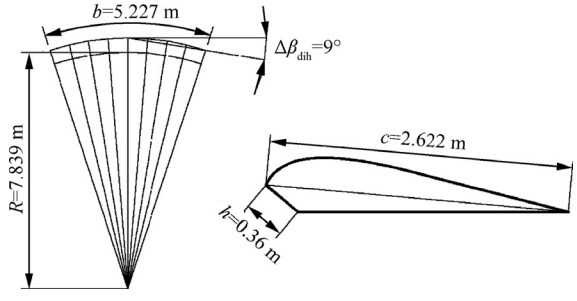

Fig. 7 Parafoil model for aerodynamic validation.

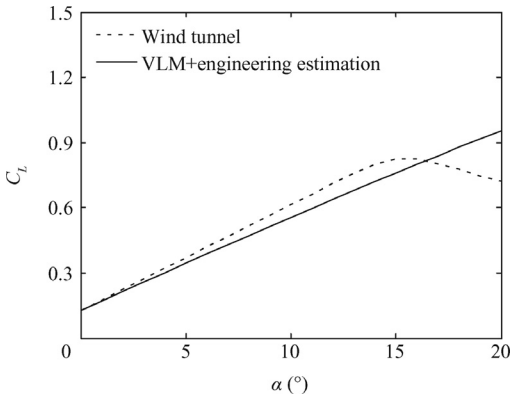

Fig. 8 Lift coefficients of aerodynamic validation.

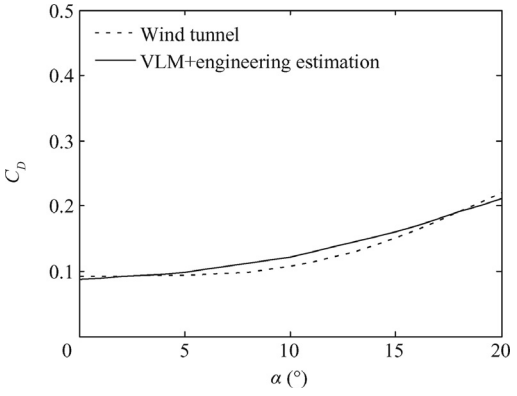

Fig. 9 Drag coefficients of aerodynamic validation.

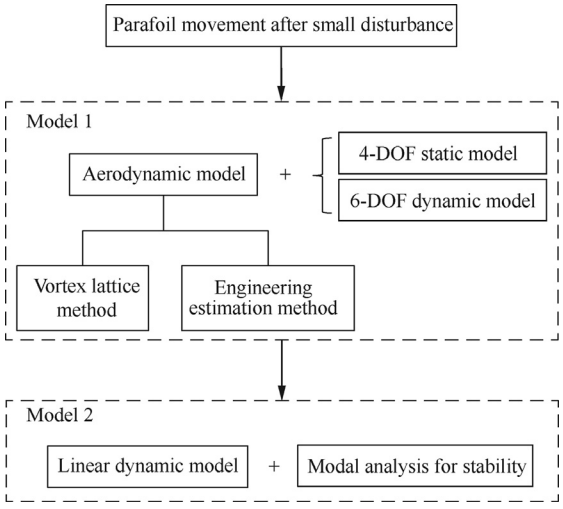

Fig. 10 Stability analysis process.

Fig. 11 shows that l_{O1O2} has little influence on longitudinal mode 1 and lateral mode 1 but has a significant effect on longitudinal mode 2 and lateral mode 2. When l_{O1O2} decreases,

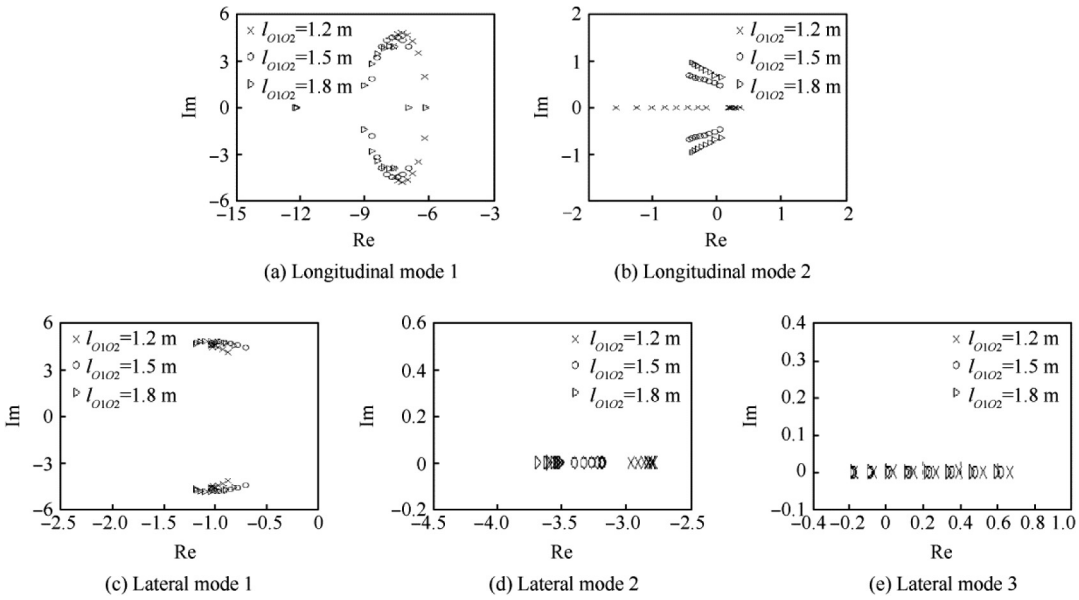

Fig. 11 Root locus with different l_{O1O2}.

the eigenvalues of longitudinal mode 2 will degenerate into two real roots and one of them may be positive. The decreasing of l_{O1O2} leads to a lower convergence rate of lateral mode 2. Although l_{O1O2} has little influence on lateral mode 3 on a small climbing angle, its reduction results in a faster divergence rate of lateral mode 3 on a large climbing angle. In other words, moderately increasing l_{O1O2} is good for the parafoil stability.

From Fig. 12, though η has a significant influence on longitudinal mode 1 and lateral mode 1, it cannot change the modes' convergence properties completely. Although η has little effect on lateral mode 2, η has a complex influence on longitudinal mode 2. If η decreases, the divergence rate of longitudinal mode 2 will first slow down, and then its eigenvalues will degenerate into real roots. Although η has little influence on lateral mode 3 on a large climbing angle, its reduction results in a slower divergence rate of lateral mode 3 on a small climbing angle. In other words, moderately decreasing η is good for parafoil stability.

5.2. Dihedral angle of canopy

It can be observed from Fig. 13 that $\Delta\beta_{\text{dih}}$ has little influence on the longitudinal modes, but it has significant effects on the lateral modes. A large canopy dihedral angle leads to not only a more stable lateral mode 1 and lateral mode 3 but also a slower convergence rate of lateral mode 2. With a small disturbance of $\Delta\beta_{\text{dih}}$, it is difficult to change the convergence properties of longitudinal mode 1 and longitudinal mode 2.

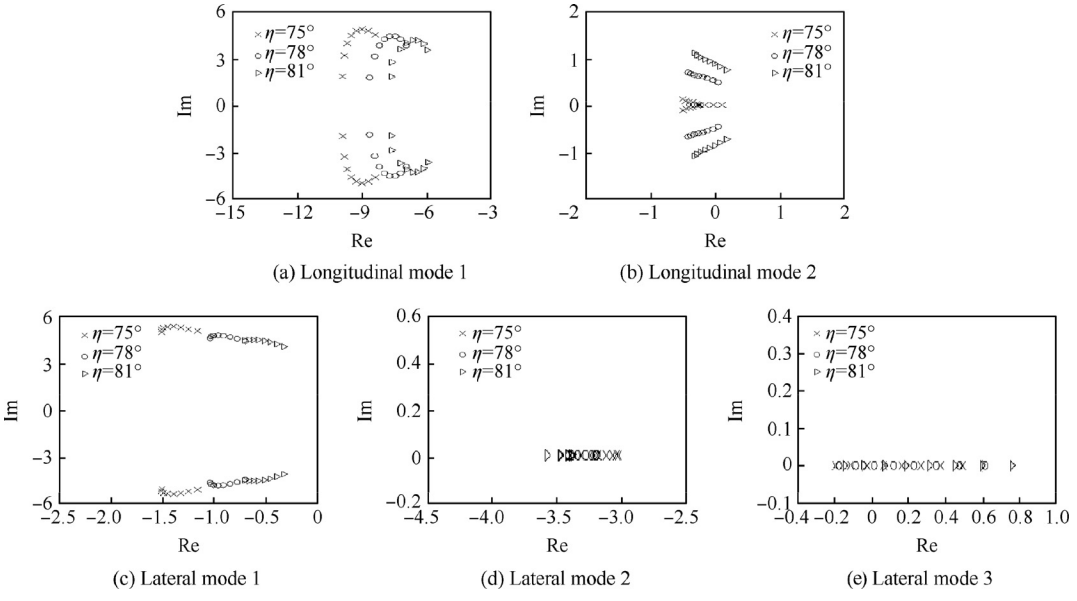

Fig. 12 Root locus with different η.

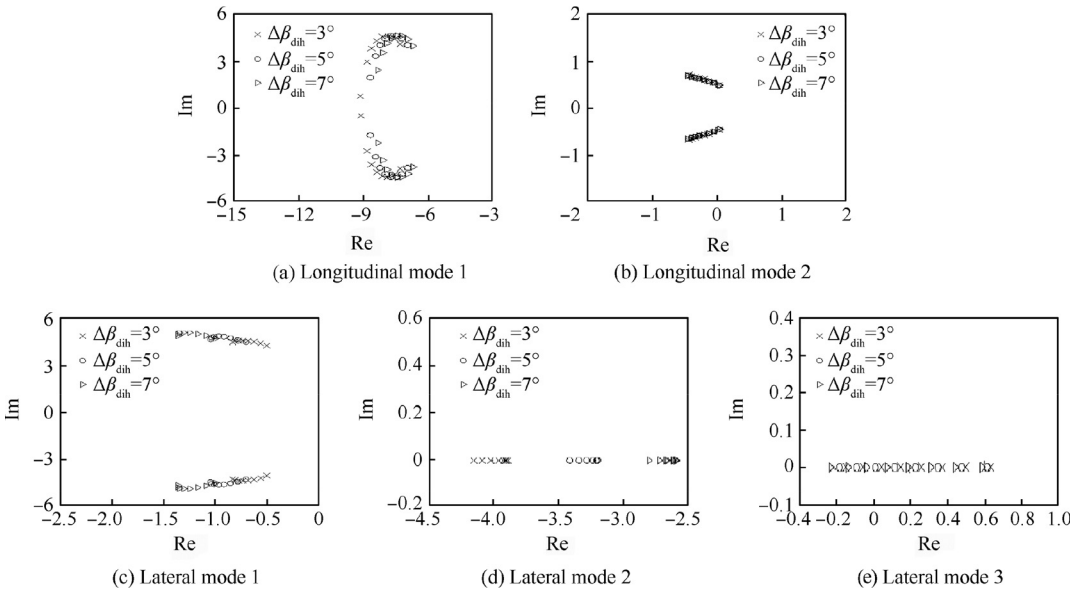

Fig. 13 Root locus with different $\Delta\beta_{dih}$.

In other words, increasing $\Delta\beta_{dih}$ is good for most of the lateral modes, especially when the divergence problem of lateral mode 3 is solved.

6. Conclusions

Parafoil motion modes are very similar to those of conventional fixed wing airplanes, including two longitudinal modes and three lateral modes. Not only longitudinal stability but also lateral stability will worsen when the climbing angle increases, and will be optimized when the geometrical parameters change. Increasing the distance between the canopy centroid and the payload centroid, decreasing the angle between the canopy-payload centroid connection line and the horizontal line, or increasing the canopy dihedral angle is good for parafoil stability.

With the 4-DOF longitudinal static model, the parafoil steady motion state was solved in this paper considering the relative motion of the canopy and the payload. Then, a 6-DOF linear dynamic model was established to analyze the modal composition, modal characteristics and motion stability. The dynamic model and solving process not only lead to conclusions which support the phenomenon that decreased stability occurs in flight climbing, but also propose a rapid stability estimate method that can be used in parafoil dynamic characteristic analysis and parafoil design.

References

1. Goodrick TF. Scale effects on performance of ram air wings. Reston(VA): AIAA; 1984. Report No.: AIAA-1984-0783.
2. Goodrick TF. Simulation studies of the flight dynamics of gliding parachute systems. Reston(VA): AIAA; 1979. Report No.: AIAA-1979-0417.
3. Goodrick TF. Theoretical study of the longitudinal stability of high-performance gliding airdrop systems. Reston(VA): AIAA; 1975. Report No.: AIAA-1975-1394.
4. Nicolaides JD. Parafoil wind tunnel tests. 1971. Report No.: AD731564.
5. Nicolaides JD. Parafoil flight performance. Reston(VA): AIAA; 1970. Report No.: AIAA-1970-1190.
6. Redelinghuys C, Rhodes SC. A graphic portrayal of parafoil trim and static stability. Reston(VA): AIAA; 2007. Report No.: AIAA 2007–2561.
7. Benedetti DM, de Freitas Pinto RLU, Ferreira RPM. Paragliders stability characteristics. Warrendale(PA): SAE International; 2013. Report No.: 2013-36-0355.
8. Ward M, Culpepper S, Costello M. Parametric study of powered parafoil flight dynamics. Reston(VA): AIAA; 2012. Report No.: AIAA-2012-4726.
9. Drozd V, Johnson P. Gliding parachute performance testing. Reston(VA): AIAA; 2001. Report No.: AIAA 2001–2016.
10. Iosilevskii G. Center of gravity and minimal lift coefficient limits of a gliding parachute. *J Aircraft* 1995;**32**(6):1297–302.
11. Crimi P. Lateral stability of gliding parachutes. *J Guid, Control, Dynam* 1990;**13**(6):1060–3.
12. Zhang H, Chen Z, Qiu J. Modeling and motion analysis of multi-bodies dynamic of unmaned parafoil vehicle. *J Syst Simul* 2016;**28**(8):1841–5 [Chinese].
13. Yu G. Nine-degree of freedom modeling and flight dynamic analysis of parafoil aerial delivery system. *Proc Eng* 2015;**99**:866–72.
14. Zhu EL, Sun QL, Tan PL, Chen ZQ, Kang XF, He YP. Modeling of powered parafoil based on Kirchhoff motion equation. *Nonlinear Dynam* 2015;**79**(1):617–29.
15. Luders B, Ellertson A, How JP, Sugel I. Wind uncertainty modeling and robust trajectory planning for autonomous parafoils. *J Guid, Control, Dynam* 2016;**39**(7):1614–30.
16. Chiel BS, Dever C. Autonomous parafoil guidance in high winds. *J Guid, Control, Dynam* 2015;**38**(5):963–9.
17. Scheuermann E, Ward M, Cacan MR, Costello M. Combined lateral and longitudinal control of parafoils using upper-surface canopy spoilers. *J Guid, Control, Dynam* 2015;**38**(11):2122–31.
18. Melin T. *A vortex lattice MATLAB implementation for linear aerodynamic wing applications [dissertation]*. Stockholm, Sweden: Royal Institute of Technology; 2000.
19. Song L, Yang H, Zhang Y, Zhang HY, Huang J. Dihedral influence on lateral-directional dynamic stability on large aspect

ratio tailless flying wing aircraft. *Chin J Aeronaut* 2014;**27**(5):1449–55.
20. Song L, Yang H, Yan XF, Ma C, Huang J. A study of instability in a miniature flying-wing aircraft in high-speed taxi. *Chin J Aeronaut* 2015;**28**(3):749–56.
21. Lingard JS. The aerodynamics of gliding parachutes. Reston(VA): AIAA; 1986. Report No.: AIAA-1986-2427.
22. Lissaman PBS, Brown GJ. Apparent mass effects on parafoil dynamics. Reston(VA): AIAA; 1993. Report No.: AIAA-1993-1236.
23. Yang H, Song L, Liu C, Huang J. Study on powered-parafoil longitudinal flight performance with a fast estimation model. *J Aircraft* 2013;**50**(5):1660–8.